Design and Analysis of a CPT System With Extendable Pairs of Electric Field Couplers

Wei Zhou, *Member, IEEE*, Qiao Gao, Ruikun Mai, *Senior Member, IEEE*, Zhengyou He, *Senior Member, IEEE*, and Aiguo Patrick Hu, *Senior Member, IEEE*

***Abstract*—The demand for wireless power transfer systems at different power levels has been increasing for various applications, and this requires power converters with different capacities. This article proposes a capacitive power transfer (CPT) system that can be extended by a modularized approach with multiple electric field couplers. A dual-input dual-output (DIDO) system with four pairs of coupling plates is studied in detail, and it is found that the complicated cross coupling between the plates is a major barrier affecting the resonance and power transfer performance of the system. In this article, the effect of mutual capacitances on the system resonance is analyzed based on a general mutual coupling model of a multiple-input multiple-output electric field coupler. A decoupling circuit based on shared inductances and the corresponding compensation network are proposed and designed. The example system with a DIDO coupler is regarded as an extension by doubling the single-input single-output (SISO) couplers via appropriate double-sided compensation. A 1.5-kW CPT system with a DIDO coupler is built by paralleling two systems with SISO couplers, and the experimental results show that the output power doubles that of the system with the SISO coupler, so the effectiveness of the modular design approach is validated.**

***Index Terms*—Capacitive power transfer (CPT), dual-input dual-output (DIDO), modular design, shared decoupling inductance.**

I. Introduction

CAPACITIVE power transfer (CPT) is a new type of wireless power transfer (WPT) technology, which uses metal plates (foils) as the coupler and a high-frequency electric field as the power transfer medium [1]–[4]. CPT and inductive power transfer (IPT) are the two most popular near-field WPT technologies at present. The electric field coupler of CPT systems has the advantages of higher plasticity, reduced volume, and reduced weight. The potential application scenarios for CPT systems are gradually increasing, including implanted biomedical devices [5], mobile phones [6], unmanned aerial vehicles [7], and motors [8], among others.

There is an increasing need for developing WPT systems at different power levels. Taking the wireless charging of electric vehicles (EVs) as an example, a variety of power levels are required for different EVs, such as e-cars and e-buses. Among the existing wireless charging standards for EVs, SAE-J2954 defines four power levels of 3.7, 7.7, 11.1, and 22 kVA [9], and GB/T-38775 provides seven different power levels covering 3.7–66 kW [10]. However, in response to the charging requirements of various power levels, converters with different power capabilities need to be repeatedly designed; hence, the R&D cost becomes higher. A modularized WPT design approach can provide an effective solution. It would be desirable to design standard WPT modular units with an appropriate power capability first and then combine the modules to flexibly meet different levels of power requirements.

In the existing literature, most of the research on modularized WPT systems for different applications is based on IPT technology, which can be divided into three categories: systems with multilevel converters, parallel converters, and multiple power transfer channels.

In the WPT system with the multilevel converter, a multilevel inverter with phase-shifting control is used as an equivalent ac voltage source of the IPT system [11], [12]. In this method, the input current of the system is equal to the current of each inverter, while the input voltage of the system is equally borne by multiple inverters. Therefore, the power capability of the multilevel inverter can be increased by increasing the number of modularized inverter modules. Besides, power transfer capacity of IPT systems can also be enhanced by paralleling multiple modularized inverters [13], [14]. The output currents of inverter modules are superimposed by using a current balance controller.

The existing multilevel and parallel converters are helpful for improving the flexibility to meet different power requirements of IPT systems. However, these two types of converters still have some shortcomings: the inverter units of the multilevel converter are connected in series, so a failure of one inverter

Manuscript received July 12, 2021; revised October 15, 2021; accepted December 9, 2021. Date of publication December 13, 2021; date of current version February 18, 2022. This work was supported in part by the National Natural Science Foundation of China under Grant 51907170 and in part by Sichuan Science and Technology Program under Grant 2021YFH0039. Recommended for publication by Associate Editor K. Akatsu. *(Corresponding authors: Zhengyou He; Aiguo Patrick Hu.)*

Wei Zhou, Qiao Gao, Ruikun Mai, and Zhengyou He are with the Key Laboratory of Magnetic Suspension Technology and Maglev Vehicle, Ministry of Education, School of Electrical Engineering, Southwest Jiaotong University, Chengdu 610031, China (e-mail: wzhou@swjtu.edu.cn; gaoq1221@163.com; mairk@swjtu.edu.cn; hezy@swjtu.edu.cn).

Aiguo Patrick Hu is with the Department of Electrical, Computer and Software Engineering, University of Auckland, Auckland 1142, New Zealand (e-mail: a.hu@auckland.ac.nz).

Color versions of one or more figures in this article are available at https://doi.org/10.1109/TPEL.2021.3134708.

Digital Object Identifier 10.1109/TPEL.2021.3134708

will lead to the whole system failing, and the reliability of the system is relatively lower [15]. The main problem with parallel converters is the serious circulating current due to the asymmetry of the inverter parameters. Although there are some circulating current suppression methods, these increase the cost and size of the system [16].

Compared with the two methods above, constructing multiple power transfer channels by combining several modularized IPT systems with a single-input single-output (SISO) coupler also helps to flexibly increase the system power capacity. Hence, the multiple-input multiple-output (MIMO) coupler is designed and applied to the IPT systems [17]. However, due to the limited volume of the coupler, there are same-side couplings between multiple transmitting coils as well as between the receiving coils. The mutual inductances between the same-side coils can cause system detuning, and simply combining multiple modularized IPT systems with a SISO coupler cannot achieve the superposition of active power [18]. At present, there are several methods on the same-side decoupling for IPT systems, such as additional capacitances [19], shared capacitances [20], and decoupled coils [21], [22].

Similarly, the MIMO electric field coupler also has the mutual capacitances between the same-side metal plates, which can affect the resonance of the CPT system [23]. The existing studies show that the intermodule interactions in a CPT system with MIMO electric field couplers can be eliminated by forcing the voltages at the same-side coupling plates in each module to be equal in magnitude but opposite in phase [24]. However, an important premise of this decoupling method is that the circuits of the two modules need to be symmetrical, which may not be easy to realize in a practical design.

To address that research gap, this article proposes a CPT system that can be extended by a modularized approach with multiple pairs of electric field couplers to meet different levels of power requirements. A mathematical model and an equivalent circuit of the MIMO electric field coupler are established in Section II, and a dual-input dual-output (DIDO) electric field coupler composed of eight plates selected as an example. The influence of the same-side mutual capacitances on the system resonance is analyzed, and a decoupling method based on a shared inductance and an $LCLCL$ compensation network is proposed and analyzed in Section III. In Section IV, the parametric design method of the system is given, and a comparison analysis is made between the proposed system and a CPT system with the SISO coupler. An experimental setup is constructed in Section V to verify the effectiveness of the modular design approach. Finally, Section VI concludes this article.

II. Model of Electric Field Coupler With Multiports

A. Overview of the Proposed CPT System

Fig. 1 shows the structure of a CPT system with a DIDO electric field coupler. The electric field coupler is composed of two pairs of transmitting plates and two pairs of receiving plates.

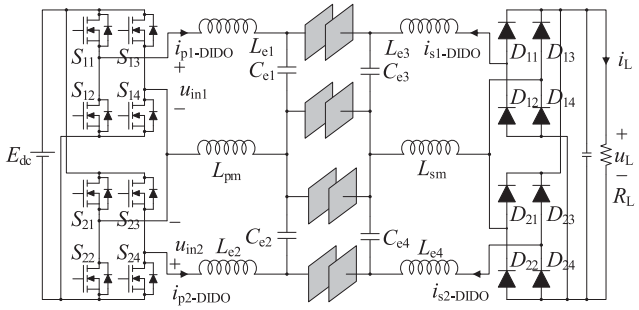

Fig. 1. Circuit diagram of the CPT system with a DIDO electric field coupler.

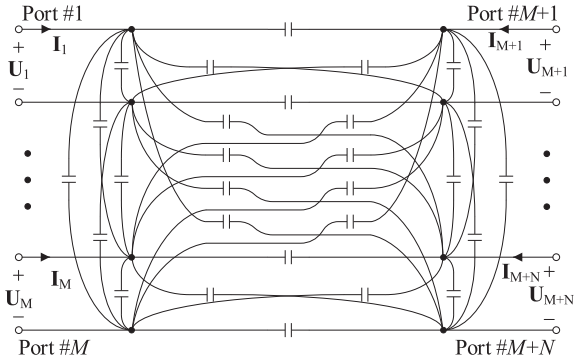

Fig. 2. Capacitances between the metal plates of the MIMO electric field coupler with M input ports and N output ports.

At the primary side, the dc voltage E_{dc} is converted to a high-frequency ac voltage by two full-bridge inverters, and the input ports of the inverters are connected with E_{dc} in parallel. At the secondary side, two full-bridge rectifiers are used to convert the high-frequency ac voltage into a dc output voltage to drive the load R_L. Similar to most CPT systems with a SISO coupler, each electric field coupler presents a large capacitive reactance, so the system needs compensation to ease the power flow. The LC compensation networks before and after the electric field coupler shown in Fig. 1 can be regarded as having two separate input and output ports.

B. Voltage and Current Relationship of the DIDO Coupler

In [23], a general mutual coupling model of the MIMO electric field coupler with an arbitrary number of ports was proposed. The capacitances between all the plates of the MIMO system are considered in this model. In addition, environmental factors, such as surrounding metal foreign objects and the earth, can also be considered as additional metal plates if their effects cannot be ignored. To generalize, a MIMO electric field coupler network with M input ports and N output ports is illustrated in Fig. 2.

According to the superposition theorem, the relationship between the port voltages and port currents of the MIMO electric field coupler can be expressed as a matrix equation

$$\mathbf{U} = \mathbf{Z} \cdot \mathbf{I} \tag{1}$$

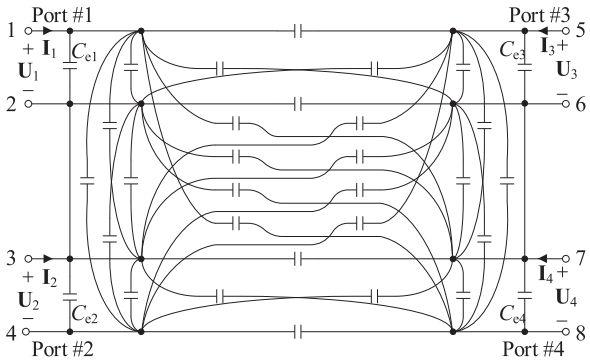

Fig. 3. Capacitance network circuit of the DIDO electric field coupler.

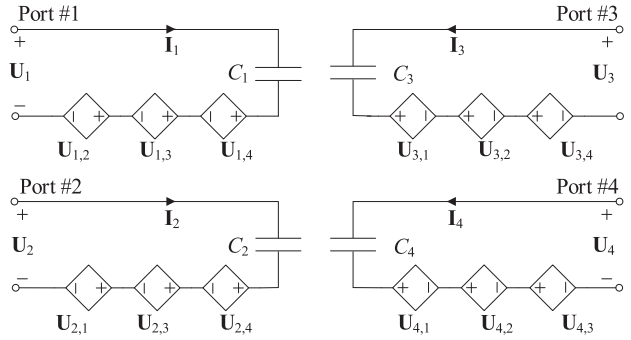

Fig. 4. Equivalent circuit of the DIDO electric field coupler.

where

$$\mathbf{U} = \begin{bmatrix} \mathbf{U}_1 \cdots \mathbf{U}_i \cdots \mathbf{U}_{M+N} \end{bmatrix}^T$$

$$\mathbf{I} = \begin{bmatrix} \mathbf{I}_1 \cdots \mathbf{I}_j \cdots \mathbf{I}_{M+N} \end{bmatrix}^T$$

$$\mathbf{Z} = \frac{1}{j\omega} \cdot \begin{bmatrix} C_{11}^{*-1} & \cdots & C_{1j}^{*-1} & \cdots & C_{1,M+N}^{*-1} \\ \vdots & \ddots & \vdots & \ddots & \vdots \\ C_{i1}^{*-1} & \cdots & C_{ij}^{*-1} & \cdots & C_{i,M+N}^{*-1} \\ \vdots & \ddots & \vdots & \ddots & \vdots \\ C_{M+N,1}^{*-1} & \cdots & C_{M+N,j}^{*-1} & \cdots & C_{M+N,M+N}^{*-1} \end{bmatrix}$$

and ω represents the angular frequency. All the elements C_{ij}^* can be calculated using this model. When $i = j$, C_{ij}^* is defined as the self-capacitance of the port i or j, and C_{ij}^* is rewritten as C_i. When $i \neq j$, C_{ij}^* is defined as the mutual capacitance of the port i and j, and C_{ij}^* is rewritten as C_{mij}.

For a DIDO system with eight coupling plates, as shown in Fig. 1, its electric field coupling can be represented by a circuit diagram shown in Fig. 3, which is consistent with the general MIMO model (see Fig. 2) when both the input and output port numbers are two. In the modeling process of the electric field coupler, there are two points that should be noted.

1) Due to the extremely small value of the permittivity ϵ_0, the self-capacitance of the coupler is also small. The values of compensation inductance become large, which result in a larger volume and internal resistance. Therefore, similar to most CPT systems with a SISO coupler, external capacitors C_{e1}–C_{e4} are connected in parallel with the ports to increase the self-capacitances. Because the external capacitors are connected with the capacitances shown in Fig. 3, C_{e1}–C_{e4} should be considered as part of the coupler for unified analysis in coupler modeling and equivalent circuit construction.
2) In Fig. 3, the primary plates 2 and 3 are connected directly, as are the secondary plates 6 and 7. In the process of modeling the coupler, the branch admittances between these plates are all set to infinity, instead of relying on the capacitances between the plates.

According to (1), the relationship between the port voltages and currents of the DIDO electric field coupler is given as

$$\underbrace{\begin{bmatrix} \mathbf{U}_1 \\ \mathbf{U}_2 \\ \mathbf{U}_3 \\ \mathbf{U}_4 \end{bmatrix}}_{\mathbf{U}} = \frac{1}{j\omega} \cdot \underbrace{\begin{bmatrix} C_1^{-1} & C_{m12}^{-1} & C_{m13}^{-1} & C_{m14}^{-1} \\ C_{m12}^{-1} & C_2^{-1} & C_{m23}^{-1} & C_{m24}^{-1} \\ C_{m13}^{-1} & C_{m23}^{-1} & C_3^{-1} & C_{m34}^{-1} \\ C_{m14}^{-1} & C_{m24}^{-1} & C_{m34}^{-1} & C_4^{-1} \end{bmatrix}}_{\mathbf{Z}} \underbrace{\begin{bmatrix} \mathbf{I}_1 \\ \mathbf{I}_2 \\ \mathbf{I}_3 \\ \mathbf{I}_4 \end{bmatrix}}_{\mathbf{I}}. \quad (2)$$

C. Equivalent Circuit of the DIDO Electric Field Coupler

According to (2), the expression of any port voltage can be deduced as follows:

$$\mathbf{U}_i = \frac{1}{j\omega C_i} \cdot \mathbf{I}_i + \sum_{j \in [1,4], j \neq i} \frac{1}{j\omega C_{mij}} \cdot \mathbf{I}_j \quad (3)$$

where the port voltage $\mathbf{U}_i$ is composed of two parts. The first part refers to the voltage on the self-capacitor C_i and the second indicates the induced voltage stimulated by the cross coupling. The expression of the induced voltage on port i excited by the current in port j can be expressed as

$$\mathbf{U}_{i,j} = \frac{1}{j\omega C_{mij}} \cdot \mathbf{I}_j. \quad (4)$$

Substituting (4) into (3), the expression of any port voltage can be rewritten as

$$\mathbf{U}_i = \frac{1}{j\omega C_i} \cdot \mathbf{I}_i + \sum_{j \in [1,4], j \neq i} \mathbf{U}_{i,j}. \quad (5)$$

According to (5), the DIDO electric field coupler in Fig. 3 can be transformed into the equivalent circuit in Fig. 4.

In Fig. 4, the complicated capacitance network circuit of the DIDO electric field coupler in Fig. 3 is equivalent to four simple series circuits, and each series circuit comprises a self-capacitance C_i and three current-controlled voltage sources (CCVS). This is an important basis for the design of same-side decoupling and compensation circuit in the following sections.

III. Same-Side Decoupling and Compensation Network

Similar to the CPT system with a SISO electric field coupler, the voltage and current of inverters in the proposed system should be in-phase through a proper compensation network design, so as to reduce the reactive power and realize the soft

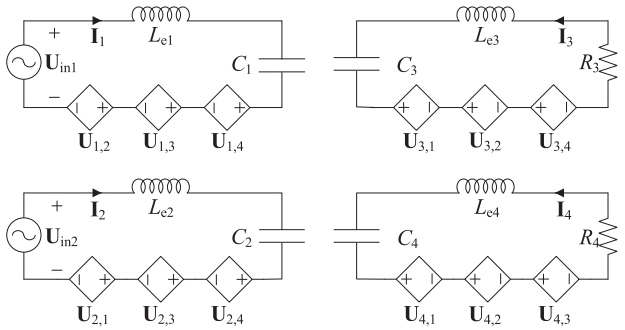

Fig. 5. Equivalent circuit of the CPT system with a DIDO electric field coupler without considering the decoupling inductances.

switching. In addition, it is necessary to eliminate the mutual capacitances on both sides of the system, since the mutual capacitances between the ports on the same side of coupler affect the voltage and current phase of the inverter.

A. Influence of Same-Side Mutual Capacitance on Resonance

Four LC circuits (L_{e1}, C_{e1}), (L_{e2}, C_{e2}), (L_{e3}, C_{e3}), and (L_{e4}, C_{e4}) compensate the DIDO electric field coupler, as shown in Fig. 1. Assuming the decoupling inductances L_{pm} and L_{sm} are not added, the equivalent circuit of the proposed system can be given in Fig. 5 according to (2). In Fig. 5, $\mathbf{U}_{\text{in1}}$ and $\mathbf{U}_{\text{in2}}$ are the voltage sources of the two inverters, and R_3 and R_4 are the equivalent resistances of the two rectifiers.

In Fig. 5, when the self-capacitances C_{e1}–C_{e4} are fully tuned with compensation inductances L_{e1}–L_{e4}, the circuit can be described by Kirchhoff's voltage law (KVL) equation as

$$\frac{1}{j\omega}\cdot\begin{bmatrix} 0 & C_{m12}^{-1} & C_{m13}^{-1} & C_{m14}^{-1} \\ C_{m12}^{-1} & 0 & C_{m23}^{-1} & C_{m24}^{-1} \\ C_{m13}^{-1} & C_{m23}^{-1} & j\omega R_3 & C_{m34}^{-1} \\ C_{m14}^{-1} & C_{m24}^{-1} & C_{m34}^{-1} & j\omega R_4 \end{bmatrix}\cdot\begin{bmatrix} \mathbf{I}_1 \\ \mathbf{I}_2 \\ \mathbf{I}_3 \\ \mathbf{I}_4 \end{bmatrix} = \begin{bmatrix} \mathbf{U}_{\text{in1}} \\ \mathbf{U}_{\text{in2}} \\ 0 \\ 0 \end{bmatrix}. \quad (6)$$

The impedance of each input port can be derived as

$$\begin{cases} Z_{\text{in1}} = \dfrac{\mathbf{U}_{\text{in1}}}{\mathbf{I}_1} = \dfrac{A_1 + jB_1}{C_1 + jD_1} \\ Z_{\text{in2}} = \dfrac{\mathbf{U}_{\text{in2}}}{\mathbf{I}_2} = \dfrac{A_2 + jB_2}{C_2 + jD_2} \end{cases} \quad (7)$$

where the imaginary components are expressed as

$$\begin{cases} jB_1 = \frac{2jC_{m12}^{-1}}{\omega^3}\left(R_4C_{m13}^{-1}C_{m23}^{-1} + R_3C_{m14}^{-1}C_{m24}^{-1}\right) \\ jD_1 = \frac{1}{j\omega}R_3R_4C_{m12}^{-1} + \frac{1}{j\omega^3}C_{m12}^{-1}C_{m34}^{-2} \\ \quad + \frac{jC_{m34}^{-1}}{\omega^3}\left(C_{m13}^{-1}C_{m24}^{-1} + C_{m14}^{-1}C_{m23}^{-1} - 2C_{m23}^{-1}C_{m24}^{-1}\right) \\ jB_2 = \frac{2jC_{m12}^{-1}}{\omega^3}\left(R_4C_{m13}^{-1}C_{m23}^{-1} + R_3C_{m14}^{-1}C_{m24}^{-1}\right) \\ jD_2 = \frac{1}{j\omega}R_3R_4C_{m12}^{-1} + \frac{1}{j\omega^3}C_{m12}^{-1}C_{m34}^{-2} \\ \quad + \frac{jC_{m34}^{-1}}{\omega^3}\left(C_{m13}^{-1}C_{m24}^{-1} + C_{m14}^{-1}C_{m23}^{-1} - 2C_{m13}^{-1}C_{m14}^{-1}\right). \end{cases} \quad (8)$$

Based on (7) and (8), it is proved that the imaginary component of the input impedance is caused by the existence of mutual capacitances C_{m12} and C_{m34}. When the impedance $\frac{1}{j\omega C_{m12}}$ and $\frac{1}{j\omega C_{m34}}$ are both 0, the same-side ports of the DIDO coupler are decoupled, and the voltage and current of the inverters can be in-phase only by compensating the self-capacitances of the coupler.

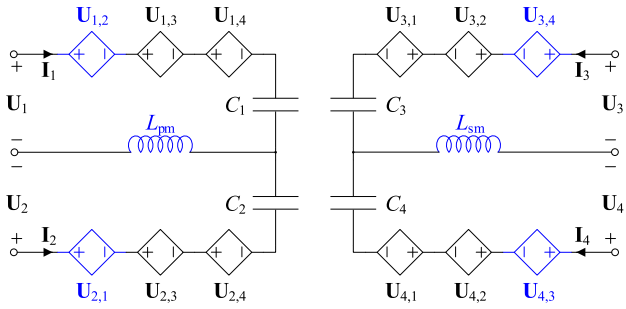

Fig. 6. Decoupling circuit of the same-side ports.

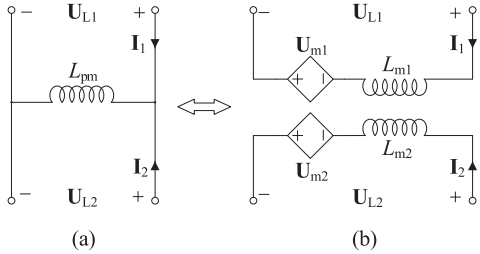

Fig. 7. Circuit transformation of the shared decoupling inductances. (a) Original circuit. (b) Equivalent circuit.

B. Decoupling of Same-Side Ports

In order to decouple the same-side coupler ports, two decoupling inductances L_{pm} and L_{sm} are added in Fig. 1. The equivalent circuit of the DIDO coupler with the decoupling inductances is illustrated in Fig. 6. In this circuit, the CCVSs $\mathbf{U}_{1,2}$, $\mathbf{U}_{2,1}$, $\mathbf{U}_{3,4}$, and $\mathbf{U}_{4,3}$ are generated due to the existence of $\frac{1}{j\omega C_{m12}}$ and $\frac{1}{j\omega C_{m34}}$. Hence, the same-side ports can be decoupled by cancelling the CCVSs above, which is realized by the shared inductors L_{pm} and L_{sm}.

Considering the shared decoupling inductance L_{pm} as a two-port network, as shown in Fig. 7(a), the relationship between port voltage and current can be expressed as

$$\begin{aligned} \begin{bmatrix} \mathbf{U}_{L1} \\ \mathbf{U}_{L2} \end{bmatrix} &= \begin{bmatrix} \mathbf{U}_{L1}/\,\mathbf{I}_1|_{\mathbf{I}_1=0} & \mathbf{U}_{L1}/\,\mathbf{I}_2|_{\mathbf{I}_2=0} \\ \mathbf{U}_{L2}/\,\mathbf{I}_1|_{\mathbf{I}_1=0} & \mathbf{U}_{L2}/\,\mathbf{I}_2|_{\mathbf{I}_2=0} \end{bmatrix}\cdot\begin{bmatrix} \mathbf{I}_1 \\ \mathbf{I}_2 \end{bmatrix} \\ &= \begin{bmatrix} j\omega L_{pm} & j\omega L_{pm} \\ j\omega L_{pm} & j\omega L_{pm} \end{bmatrix}\cdot\begin{bmatrix} \mathbf{I}_1 \\ \mathbf{I}_2 \end{bmatrix}. \end{aligned} \quad (9)$$

From (9), the circuit in Fig. 7(a) is transformed into the circuit in Fig. 7(b), where

$$\begin{cases} L_{m1} = L_{m2} = L_{pm} \\ \mathbf{U}_{m1} = j\omega L_{pm}\cdot\mathbf{I}_2 \\ \mathbf{U}_{m2} = j\omega L_{pm}\cdot\mathbf{I}_1. \end{cases} \quad (10)$$

The same transformation can also be realized for the inductance L_{sm}. Then, the circuit in Fig. 6 becomes equivalent to

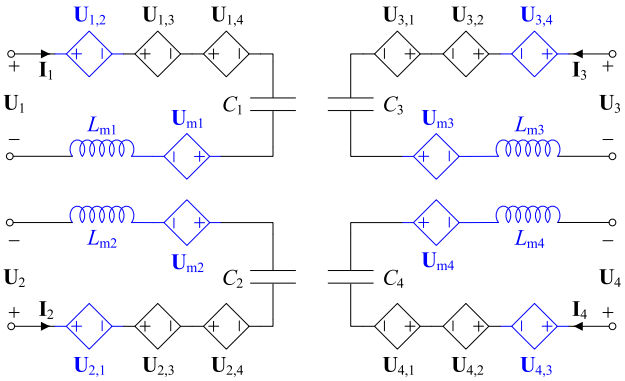

Fig. 8. Equivalent circuit of the DIDO electric field coupler with two shared decoupling inductors at both two sides.

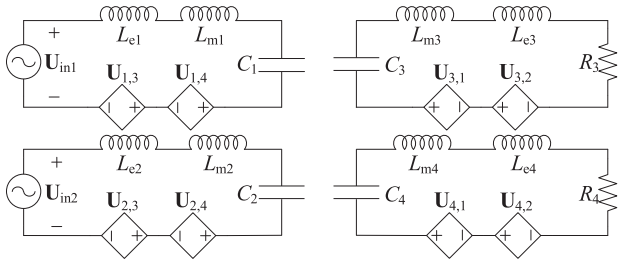

Fig. 9. Equivalent circuit of the compensated CPT system.

Fig. 8, where the parameters are given in (10) and (11)

$$\begin{cases} L_{m3} = L_{m4} = L_{sm} \\ \mathbf{U}_{m3} = j\omega L_{sm} \cdot \mathbf{I}_4 \\ \mathbf{U}_{m4} = j\omega L_{sm} \cdot \mathbf{I}_3. \end{cases} \tag{11}$$

To eliminate the CCVSs $\mathbf{U}_{1,2}, \mathbf{U}_{2,1}, \mathbf{U}_{3,4}$, and $\mathbf{U}_{4,3}$ caused by $\frac{1}{j\omega C_{m12}}$ and $\frac{1}{j\omega C_{m34}}$, the value of shared decoupling inductances L_{pm} and L_{sm} should satisfy (12) so as to decouple the same-side ports

$$\begin{cases} \mathbf{U}_{1,2} + \mathbf{U}_{m1} = 0, \mathbf{U}_{2,1} + \mathbf{U}_{m2} = 0 \\ \mathbf{U}_{3,4} + \mathbf{U}_{m3} = 0, \mathbf{U}_{4,3} + \mathbf{U}_{m4} = 0 \end{cases}$$
$$\Rightarrow \begin{cases} \omega^2 L_{pm} C_{m12} = 1 \\ \omega^2 L_{sm} C_{m34} = 1. \end{cases} \tag{12}$$

C. Double-Sided LC Compensation Circuit

After decoupling the same-side ports of the DIDO coupler, resonance of the system can be achieved only by compensating the self-capacitance and decoupling inductance. The equivalent circuit of the compensated system is shown in Fig. 9. Because L_{m1}–L_{m4} are not fully tuned with C_1–C_4, four additional compensation inductances L_{e1}–L_{e4} are connected in series with the self-capacitances. The values of L_{e1}–L_{e4} satisfy the following equation, where $k = \{1, 2, 3, 4\}$:

$$\omega^2 \left(L_{ek} + L_{mk}\right) C_k = 1. \tag{13}$$

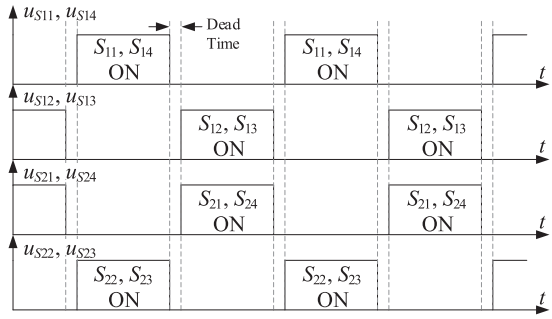

Fig. 10. Driving sequence of two full-bridge inverters.

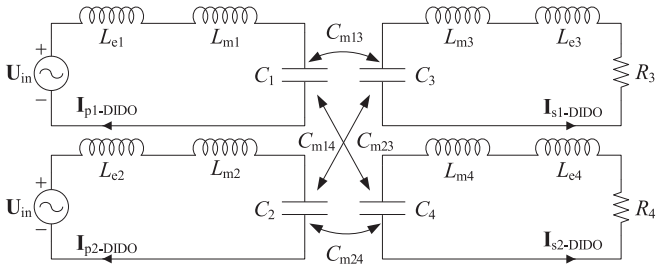

Fig. 11. Equivalent circuit of the CPT system based on the mutual capacitances.

IV. System Analysis and Design

A. Inverter Drive Sequence

As shown in Fig. 1, the input ports of two inverters are connected in parallel, and the two bridge arms are directly connected. Therefore, when S_{13} and S_{22} or S_{14} and S_{21} are switched ON at the same time, the dc power supply will be short-circuited and a current spike will be generated. In order to avoid short circuiting, the phase difference between two inverters must be 180°, and a certain dead time needs to be set to avoid short circuiting caused by coincident rising and falling time of the switches. The driving sequence of two inverters is shown in Fig. 10.

B. Power Transfer Capacity

According to the driving sequence in Fig. 10, the inverters can be equivalent to two ac sources with the same voltage $\mathbf{U}_{\text{in}} = \mathbf{U}_{\text{in1}} = \mathbf{U}_{\text{in2}}$, with the root-mean-square (RMS) value being

$$|\mathbf{U}_{\text{in}}| = \frac{2\sqrt{2}E_{\text{dc}}}{\pi}. \tag{14}$$

The input impedance of two rectifiers can be regarded as two equivalent resistors R_3 and R_4. Based on the circuit equivalence from Figs. 6–8, the system circuit in Fig. 1 can be simplified as the equivalent circuit in Fig. 11. When the circuit is fully tuned, i.e., (12) and (13) are satisfied, the proposed system can

be described by the matrix expression of KVL as follows:

$$\frac{1}{j\omega}\cdot\begin{bmatrix}0 & 0 & C_{m13}^{-1} & C_{m14}^{-1}\\ 0 & 0 & C_{m23}^{-1} & C_{m24}^{-1}\\ C_{m13}^{-1} & C_{m23}^{-1} & j\omega R_3 & 0\\ C_{m14}^{-1} & C_{m24}^{-1} & 0 & j\omega R_4\end{bmatrix}\cdot\begin{bmatrix}\mathbf{I}_{p1-\mathrm{DIDO}}\\ \mathbf{I}_{p2-\mathrm{DIDO}}\\ \mathbf{I}_{s1-\mathrm{DIDO}}\\ \mathbf{I}_{s2-\mathrm{DIDO}}\end{bmatrix}=\begin{bmatrix}\mathbf{U}_{\mathrm{in}}\\ \mathbf{U}_{\mathrm{in}}\\ 0\\ 0\end{bmatrix}. \tag{15}$$

Substituting (14) into (15), the current on the receiving side can be derived as

$$\begin{cases}|\mathbf{I}_{s1-\mathrm{DIDO}}|=\dfrac{2\sqrt{2}E_{\mathrm{dc}}\omega}{\pi}\cdot\dfrac{C_{m13}C_{m23}\left(C_{m24}-C_{m14}\right)}{C_{m13}C_{m24}-C_{m14}C_{m23}}\\ |\mathbf{I}_{s2-\mathrm{DIDO}}|=\dfrac{2\sqrt{2}E_{\mathrm{dc}}\omega}{\pi}\cdot\dfrac{C_{m14}C_{m24}\left(C_{m13}-C_{m23}\right)}{C_{m13}C_{m24}-C_{m14}C_{m23}}.\end{cases} \tag{16}$$

Hence, the current $\mathbf{I}_{L-\mathrm{DIDO}}$ on the dc load after rectification is

$$I_{L-\mathrm{DIDO}}=\frac{2\sqrt{2}}{\pi}\cdot\left(|\mathbf{I}_{s1-\mathrm{DIDO}}|+|\mathbf{I}_{s2-\mathrm{DIDO}}|\right)=\frac{8E_{\mathrm{dc}}\omega\Delta_1}{\pi^2\Delta_2} \tag{17}$$

where

$$\begin{cases}\Delta_1=C_{m13}C_{m24}(C_{m14}+C_{m23})-C_{m14}C_{m23}\left(C_{m13}+C_{m24}\right)\\ \Delta_2=C_{m13}C_{m24}-C_{m14}C_{m23}.\end{cases}$$

Then, the transfer admittance $G_{iu-\mathrm{DIDO}}$ of the CPT system with a DIDO coupler, which is the ratio of the output current to the input voltage, can be calculated according to the mutual capacitance C_{mij} of the coupler. All the mutual capacitances are affected by the geometric parameters of coupler and the external capacitances, C_{e1}–C_{e4}. Because the size of the coupler is known, the external capacitances become the only variables that affect the mutual capacitance and $G_{iu-\mathrm{DIDO}}$. In order to simplify the analysis, all the external capacitances are set to be equal. Define $C_e=C_{ek}$, where $k=\{1,2,3,4\}$. Therefore, the transfer admittance $G_{iu-\mathrm{DIDO}}$ can be given as

$$G_{iu-\mathrm{DIDO}}\left(C_e\right)=\frac{I_{L-\mathrm{DIDO}}}{E_{\mathrm{dc}}}=\frac{8\omega}{\pi^2}\cdot\frac{\Delta_1\left(C_e\right)}{\Delta_2\left(C_e\right)}. \tag{18}$$

According to the current on the dc load R_L, the equivalent ac voltage at the input of rectifiers can be derived. Combined with the ac current in (16), the equivalent resistive load R_3 and R_4 can be obtained as follows:

$$\begin{cases}R_3=\dfrac{2\sqrt{2}}{\pi}\cdot\dfrac{I_{L-\mathrm{DIDO}}R_L}{|\mathbf{I}_{s1-\mathrm{DIDO}}|}\\ R_4=\dfrac{2\sqrt{2}}{\pi}\cdot\dfrac{I_{L-\mathrm{DIDO}}R_L}{|\mathbf{I}_{s2-\mathrm{DIDO}}|}.\end{cases} \tag{19}$$

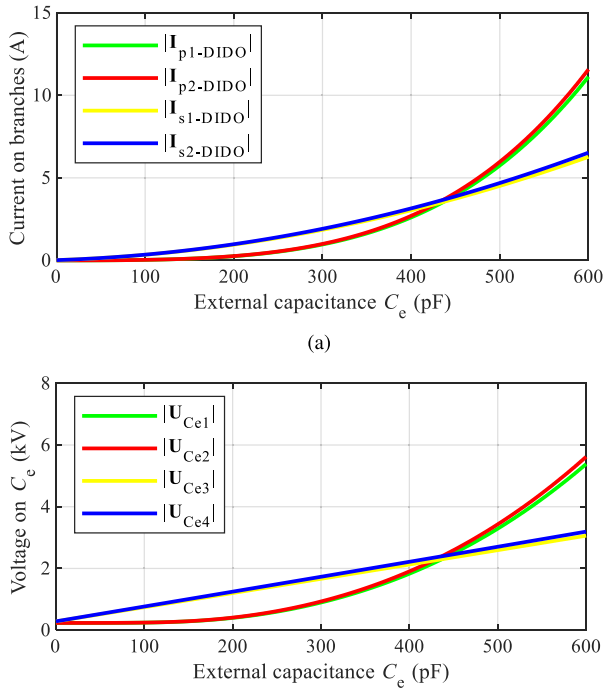

Fig. 12. Relationship between (a) branch current and (b) voltage on the external capacitors against the external capacitance C_e.

Substituting (19) into (15), the current on the primary side can be given as

$$\begin{cases}|\mathbf{I}_{p1-\mathrm{DIDO}}|=\dfrac{16\sqrt{2}E_{\mathrm{dc}}\omega^2R_L}{\pi^3}\cdot\dfrac{C_{m13}C_{m14}(C_{m24}-C_{m23})\Delta_1}{\Delta_2^2}\\ |\mathbf{I}_{p2-\mathrm{DIDO}}|=\dfrac{16\sqrt{2}E_{\mathrm{dc}}\omega^2R_L}{\pi^3}\cdot\dfrac{C_{m23}C_{m24}(C_{m13}-C_{m14})\Delta_1}{\Delta_2^2}.\end{cases} \tag{20}$$

Then, the voltage on the external capacitances of the capacitive coupler can be derived in (21), where $\mathbf{U}_{Ce1}$–$\mathbf{U}_{Ce4}$ represent the voltage on the external capacitances C_{e1}–C_{e4}. The relationship curve between the branch current and the voltage on the external capacitance $\mathbf{U}_{Ce1}$–$\mathbf{U}_{Ce4}$ against the external capacitance is shown in Fig. 12. Equation (21) shown at the bottom of this page.

C. Comparative Analysis of CPT Systems With DIDO and With SISO Electric Field Coupler

In order to verify the power enhancement of the proposed CPT system with a DIDO coupler, a comparison analysis between the

$$\begin{cases}|\mathbf{U}_{Ce1}|=\sqrt{|\mathbf{U}_{\mathrm{in}}|^2+\left[\omega\left(L_{e1}+L_{pm}\right)|\mathbf{I}_{p1-\mathrm{DIDO}}|+\omega L_{pm}|\mathbf{I}_{p2-\mathrm{DIDO}}|\right]^2}\\ |\mathbf{U}_{Ce2}|=\sqrt{|\mathbf{U}_{\mathrm{in}}|^2+\left[\omega L_{pm}|\mathbf{I}_{p1-\mathrm{DIDO}}|+\omega\left(L_{e2}+L_{pm}\right)|\mathbf{I}_{p2-\mathrm{DIDO}}|\right]^2}\\ |\mathbf{U}_{Ce3}|=\sqrt{R_3^2|\mathbf{I}_{s1-\mathrm{DIDO}}|^2+\left[\omega\left(L_{sm}+L_{e3}\right)|\mathbf{I}_{s1-\mathrm{DIDO}}|+\omega L_{sm}|\mathbf{I}_{s2-\mathrm{DIDO}}|\right]^2}\\ |\mathbf{U}_{Ce4}|=\sqrt{R_4^2|\mathbf{I}_{s2-\mathrm{DIDO}}|^2+\left[\omega L_{sm}|\mathbf{I}_{s1-\mathrm{DIDO}}|+\omega\left(L_{sm}+L_{e4}\right)|_{s2-\mathrm{DIDO}}|\right]^2}\end{cases} \tag{21}$$

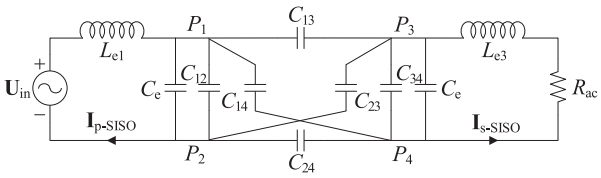

Fig. 13. Equivalent circuit of the CPT system with a SISO electric field coupler.

TABLE I
GEOMETRIC PARAMETERS OF PLATES AND PREDETERMINED CONSTANTS

Parameter	Value	Parameter	Value
l_s	550 mm	l_g	50 mm
d	30 mm	f	500 kHz
E_{dc}	260 V		

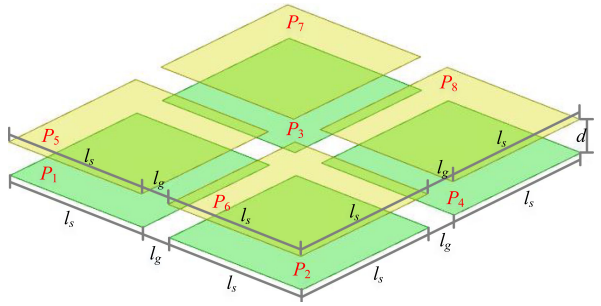

Fig. 14. DIDO electric field coupler.

proposed system and the CPT system with a SISO coupler, as shown in Fig. 13, is conducted in this section.

A double-sided LC compensation network is used in Fig. 13. The transfer admittance $G_{iu-\mathrm{SISO}}$ of the CPT system with a SISO coupler can be given as

$$G_{iu-\mathrm{SISO}}(C_s)=\frac{I_{L-\mathrm{SISO}}}{E_{\mathrm{dc}}}=\frac{8\omega}{\pi^2}\cdot\frac{C_1(C_e)\cdot C_2(C_e)-C_m^2(C_\varepsilon)}{C_m(C_e)} \tag{22}$$

where

$$\begin{cases} C_1(C_e)=C_e+C_{12}+\frac{(C_{13}+C_{14})(C_{23}+C_{24})}{C_{13}+C_{14}+C_{23}+C_{24}} \\ C_2(C_e)=C_e+C_{34}+\frac{(C_{13}+C_{23})(C_{14}+C_{24})}{C_{13}+C_{14}+C_{23}+C_{24}} \\ C_m=\frac{C_{24}C_{13}-C_{14}C_{23}}{C_{13}+C_{14}+C_{23}+C_{24}} \end{cases}$$

and $\mathbf{I}_{L-\mathrm{SISO}}$ denotes the current on the dc load and C_{ij} represents the capacitance between plates P_i and P_j of the SISO electric field coupler. The current on the primary and secondary sides can be derived as

$$\begin{cases} |\mathbf{I}_{p-\mathrm{SISO}}|=\dfrac{16\sqrt{2}E_{\mathrm{dc}}\omega^2R_L}{\pi^3}\cdot C_m^2 \\ |\mathbf{I}_{s-\mathrm{SISO}}|=\dfrac{2\sqrt{2}E_{\mathrm{dc}}\omega}{\pi}\cdot C_m. \end{cases} \tag{23}$$

In order to ensure the fairness of comparison, the following preconditions are set.

1) Two systems have the same input voltage E_{dc} and operating frequency f (as shown in Table I).

2) The DIDO coupler is composed of two SISO couplers, as shown in Fig. 14. The metal plates P_1, P_2, P_5, and P_6 form a SISO coupler, and P_3, P_4, P_7, and P_8 form another one. The dimensions of the DIDO coupler are shown in Table I.

3) Since the two output ports of the CPT system with the DIDO coupler are connected in parallel, the dc load resistance of the proposed system is set to be twice that of the CPT system with the SISO coupler to ensure that the output impedances are equal.

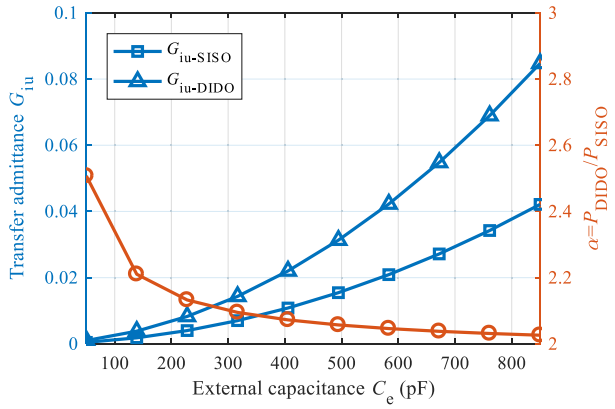

Fig. 15. Curves of transfer admittance G_{iu} and power ratio α against C_e.

According to (18) and (22), when the system frequency and the size of the coupler are determined, the transfer admittance G_{iu} of the two systems only depends on the external capacitance C_e; the relationship curves are illustrated in Fig. 15. It shows that $G_{iu-\mathrm{SISO}}$ and $G_{iu-\mathrm{DIDO}}$ are both positively correlated with the capacitance C_e. In order to compare the output power of the CPT system with DIDO and SISO couplers more intuitively, a parameter $\alpha=\frac{P_{\mathrm{DIDO}}}{P_{\mathrm{SISO}}}$ is defined as the output power ratio of the two systems, where P_{DIDO} and P_{SISO} denote the output power of the two compared systems, respectively. It can be seen from Fig. 15 that the power ratio α decreases with the increase of C_e, but is always slightly greater than 2. This shows that when the input voltage E_{dc} and the operating frequency f of the two systems are the same, the power of the CPT system with the DIDO coupler is the superposition of the power of the two CPT systems with the SISO coupler operating independently.

In addition to the output power, the primary and secondary currents of the two compared systems are also analyzed. The variables β_{p1} and β_{p2} are defined to represent the ratio of the two primary currents of the CPT system with the DIDO coupler to the primary current of the CPT system with the SISO coupler. β_{s1} and β_{s2} correspond to the ratio of the secondary currents of the two systems, respectively. In Fig. 16, the four current ratios all decrease slightly with the increase of the external capacitance C_e, but the current ratios are always near to 1. The slight asymmetry of the β curves of the two channels in Fig. 16 is mainly caused by the simulation error, especially the finite-element simulation error for the coupler. However, this error does not affect the trend and range of β curves. It proves that although the CPT system with the DIDO coupler realizes the power superposition of two CPT systems with the SISO coupler, its currents at primary and secondary sides are basically consistent with the latter system.

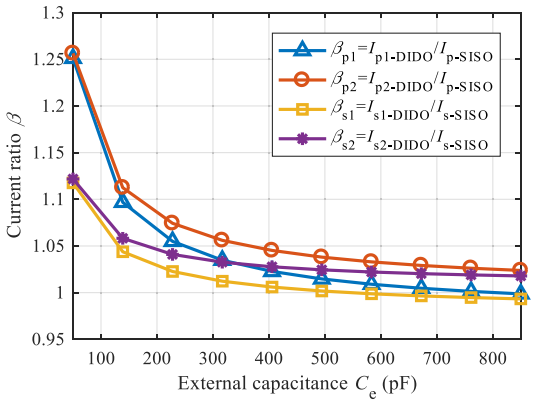

Fig. 16. Curves of current ratio of two CPT systems against capacitance C_e.

TABLE II
PARAMETERS OF THE COUPLER AND COMPENSATION NETWORK

Parameter	Value	Parameter	Value
C_1	517.41 pF	C_2	513.48 pF
C_3	517.35 pF	C_4	513.59 pF
C_{m12}	13.07 nF	C_{m13}	3.54 nF
C_{m14}	-13.33 nF	C_{m23}	-13.33 nF
C_{m24}	3.71 nF	C_{m34}	13.06 nF
L_{mp}	7.75 μH	L_{ms}	7.76 μH
L_{e1}	188.07 μH	L_{e2}	189.57 μH
L_{e3}	188.09 μH	L_{e4}	189.52 μH

D. System Parametric Design

When designing a CPT system, the size of the coupler is usually defined by the size of the installation space, so the capacitances between metal plates can be achieved using the finite-element analysis software ANSYS Maxwell. In addition, the input voltage E_{dc}, output current I_L, and the operating frequency ω are also determined in advance according to practical demands, so the external capacitance C_e can be designed using the relationship curve between the transfer admittance and the external capacitance of the proposed system, as shown in Fig. 15. After the capacitance C_e is determined, all the self-capacitances and mutual capacitances can be found from (1) and (2). Then, the shared decoupling inductances L_{pm} and L_{sm} can be calculated as (24) based on (12)

$$L_{pm} = \left(\omega^2 C_{m12}\right)^{-1}, \quad L_{sm} = \left(\omega^2 C_{m34}\right)^{-1}. \tag{24}$$

Then, the four compensation inductances are derived according to (13) as

$$\begin{aligned} L_{c1} &= \left(\omega^2 C_1\right)^{-1} - \left(\omega^2 C_{m12}\right)^{-1} \\ L_{c2} &= \left(\omega^2 C_2\right)^{-1} - \left(\omega^2 C_{m12}\right)^{-1} \\ L_{c3} &= \left(\omega^2 C_3\right)^{-1} - \left(\omega^2 C_{m34}\right)^{-1} \\ L_{c4} &= \left(\omega^2 C_4\right)^{-1} - \left(\omega^2 C_{m34}\right)^{-1}. \end{aligned} \tag{25}$$

The design flowchart of the system parameters is shown in Fig. 17. Based on the flowchart, all the main parameters are designed and listed in Table II. From the table, the following two points should be noted.

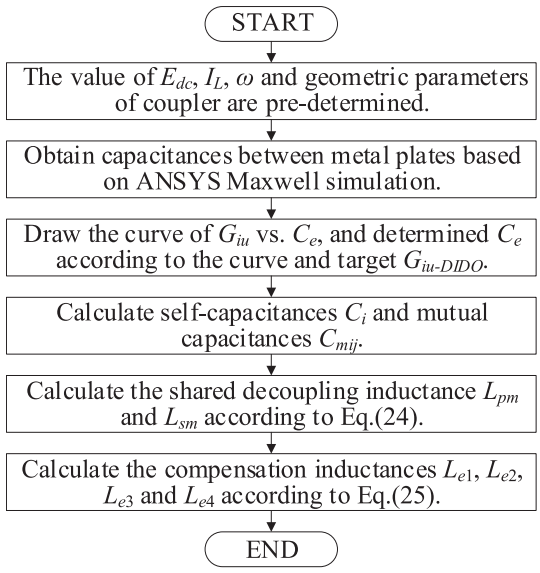

Fig. 17. Flowchart of the system parametric design.

1) The mutual capacitance is a scalar that can have positive or negative values. The mutual capacitance C_{mij} can be measured by injecting a current $\mathbf{I}_i$ into Port i and measure the open-circuit voltage $\mathbf{U}_j$ of Port j when other ports are open. The physical meaning of the positive and negative mutual capacitance C_{mij} is related to the plate coupling relationships, which can be determined by directions of the open-circuit voltage $\mathbf{U}_j$ and the excitation current $\mathbf{I}_i$. This is similar to the MIMO inductive coupler for IPT systems. The mutual inductance M may also have positive and negative values reflecting the coupling dots/directions of the coils.
2) The mutual capacitance is not positively correlated with the coupling strength. According to the model in Section II, the coupling strength between the two ports i and j is described by the mutual capacitive reactance between the ports, where the impedance is $Z_{mij} = \frac{1}{j\omega C_{mij}}$. Hence, a stronger coupling gives a smaller mutual capacitance C_{mij}.

E. Analysis of Extendable Structure

The previous sections were mainly about the design of a CPT system with a DIDO coupler. Based on the same principle, a more general extensible system can be designed. When more coupling plates are used, the cross coupling between the ports becomes more complicated. The finite-element simulation results show that the mutual capacitances between nonadjacent ports are much greater than the mutual capacitances between adjacent ports, which means that the coupling between nonadjacent ports is extremely weak and negligible. To simplify the coupler model, only the couplings between adjacent ports need to be considered.

After ignoring the mutual capacitances between nonadjacent ports, the CPT system with a general multiport electric field coupler is shown in Fig. 18. Similar to the procedure for establishing an equivalent circuit in Section III, an equivalent circuit for the

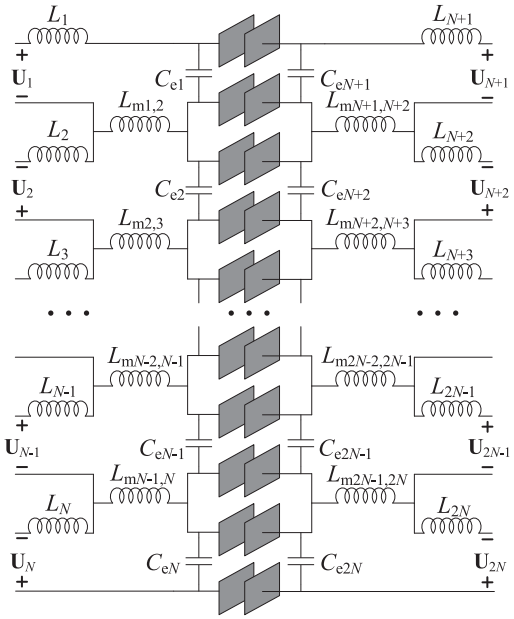

Fig. 18. Circuit diagram of the CPT system with extendable modules.

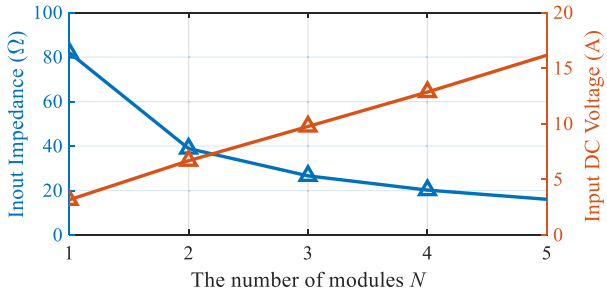

Fig. 19. Relationship curve between the input impedance and the input dc current of the whole system against the number of couplers N.

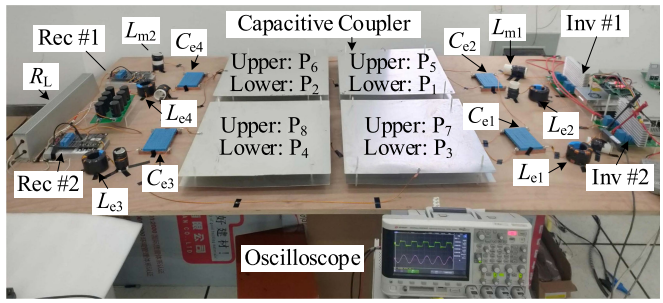

Fig. 20. Experimental setup of the proposed CPT system with a DIDO coupler.

extendable system can also be established. The main parameters of the CPT system with general expandable modules satisfy the equations as follows:

$$\begin{cases} \omega^2 \cdot (L_1 + L_{\mathrm{m}1,2}) \cdot C_1 = 1 \\ \omega^2 \cdot (L_N + L_{\mathrm{m}N-1,N}) \cdot C_N = 1 \\ \omega^2 \cdot (L_{N+1} + L_{\mathrm{m}N+1,N+2}) \cdot C_{N+1} = 1 \\ \omega^2 \cdot (L_{2\text{-}N} + L_{\mathrm{m}2N-1,2\text{-}N}) \cdot C_{2\text{-}N} = 1 \end{cases} \tag{26}$$

where C_i represents the self-capacitance of port $\#i$, and

$$\omega^2 \cdot (L_i + L_{\mathrm{m}i-1,i} + L_{\mathrm{m}i,i+1}) \cdot C_i = 1 \tag{27}$$

where $i \in \{2, \ldots, N-1\} \cup \{N+2, \ldots, 2N-1\}$, and

$$\omega^2 \cdot L_{mi,i+1} \cdot C_{mi,i+1} = 1 \tag{28}$$

where C_{mij} indicates the mutual capacitance between ports $\#i$ and $\#j$, and $i \in \{2, \ldots, N-1\} \cup \{N+2, \ldots, 2N-1\}$. According to the KVL, the system can be described as a matrix equation similar to (15). Then, the voltage and current on the component of the system can be derived by solving the matrix equation. According to the relationship between the dc input current of the inverter and the RMS value of its ac current, the curves of the input current and impedance against the number of extendable modules are obtained in Fig. 19. The curves show that the input current is almost linearly correlated with the number of modules, whereas the input impedance is inversely proportional to the number of modules.

V. Experimental Validation

A. Experimental Setup

Fig. 20 shows the experimental setup of the proposed CPT system with the DIDO electric field coupler based on the circuit shown in Fig. 1. SiC MOSFETs are adopted as switches for the two inverters $\#1$ and $\#2$ because they improve the dynamic performance and reduce the switching and conduction losses when the system operates at high frequency. Similarly, four SiC diodes are used to construct rectifiers $\#1$ and $\#2$.

The electric field coupler is composed of eight aluminum plates, the relative positions of which are fixed by nylon hex bolts. The compensation inductors are wound on ferrosilicon toroidal core with Litz wire. Compared with air-core inductors, this type of inductor has the advantages of small size, low environmental sensitivity, and minimal electromagnetic interference. Based on the experimental measurement, the losses of both types of inductor are similar. The compensation capacitors are film capacitors; each capacitor module is formed by multiple capacitor elements in series and parallel to achieve the required capacitance value and increase its voltage tolerance. The main parameters of the system are calculated according to (24) and (25) and are listed in Table II. Two experiments are conducted in this section: one is to verify the decoupling of the DIDO coupler, and the other is to demonstrate the power transfer of the whole CPT system.

B. Experimental Verification of Same-Side Decoupling

According to the finite-element simulation results and an equivalent circuit model of the electric field coupler, there is a mutual capacitance between the ports on the same side of the system, which affects the resonance of the CPT system. In Section III, a shared decoupling inductor is used to achieve decoupling between ports on the same side. In order to verify the effectiveness of the proposed decoupling method, a decoupling experiment was carried out, as illustrated in Fig. 21.

In Fig. 21(a), the secondary circuit is disconnected. The circuit is excited by an inverter with the voltage of $\mathbf{U}_{s1}$. Then, the sum of

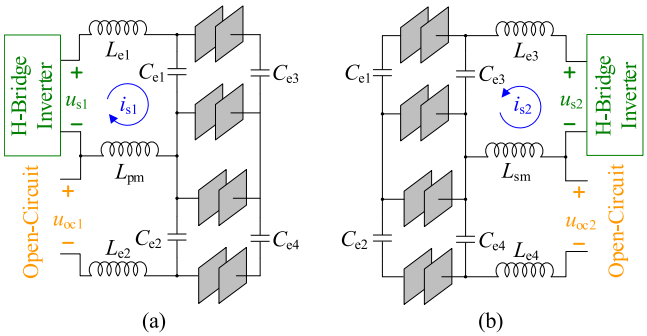

Fig. 21. Experimental verification of same-side decoupling of (a) primary side and (b) secondary side of the DIDO coupler.

the voltages on the decoupling inductance L_{pm} and the external capacitor C_{e2}, defined as $\mathbf{U}_{oc1}$, is measured with a voltage probe. According to (11), the open-circuit voltage $\mathbf{U}_{\rm oc1}$ is excited by the current $\mathbf{I}_{s1}$ and can be found from (29). Based on (12), $\mathbf{U}_{\rm oc1} = 0$ would indicate that the two ports of the primary circuit are decoupled. Similarly, the decoupling of the secondary-side circuit can be verified, as shown in Fig. 21(b). The inverter shown in Fig. 21 is to provide excitation currents $\mathbf{I}_{s1}$ and $\mathbf{I}_{s2}$ in the resonant circuits

$$\mathbf{U}_{\rm oc1} = (j\omega L_{pm} + 1/j\omega C_{m12}) \cdot \mathbf{I}_{s1} = 0 \tag{29}$$

$$\mathbf{U}_{\rm oc2} = (j\omega L_{sm} + 1/j\omega C_{m34}) \cdot \mathbf{I}_{s2} = 0. \tag{30}$$

The experimental waveforms of the circuit in Fig. 21 are presented in Fig. 22. In Fig. 22(a), the input dc voltage of the inverter is 10 V. Since the primary circuit is in resonance, the primary current $\mathbf{I}_{s1}$ and $\mathbf{U}_{s1}$ are in phase. The fundamental component of $\mathbf{U}_{\rm oc1}$ is approximately 0, and there are only some switching ripples. This verifies the correctness of the decoupling method of the primary-side port. Similarly, Fig. 22(b) shows the experimental waveforms of the secondary side, and the results are consistent with Fig. 22(a).

C. Power Transfer Performance

After the same-side ports are decoupled, the CPT system with a DIDO coupler can operate in resonance after proper compensation. The final circuit to demonstrate the power transfer performance of the whole system is the same as what was shown in Fig. 1. Fig. 23 presents the voltage and current waveforms of the experimental setup when the load resistance is 40 Ω and the output power is 1.5 kW. In Fig. 23(a), the inverter output voltage and current waveform is given. The current $i_{p1-\rm DIDO}$ of inverter #1 lags behind the voltage $u_{\rm in1}$ slightly, but the two remain basically in phase. Inverter #2 also gives the same result. For the MOSFETs of two inverters, a reasonable phase difference can make the current flow through the reverse diode when the switch is turned ON so that the source–drain voltage of the switch is 0 V and the inverter can work in soft switching status. Fig. 23(b) shows the output voltage waveform of the system.

In order to measure the output current, power, and efficiency of the system more accurately, a power analyzer HIOKI PW6001 was used, and the results are shown in Fig. 24. $U_{\rm dc1}$, $I_{\rm dc1}$, and

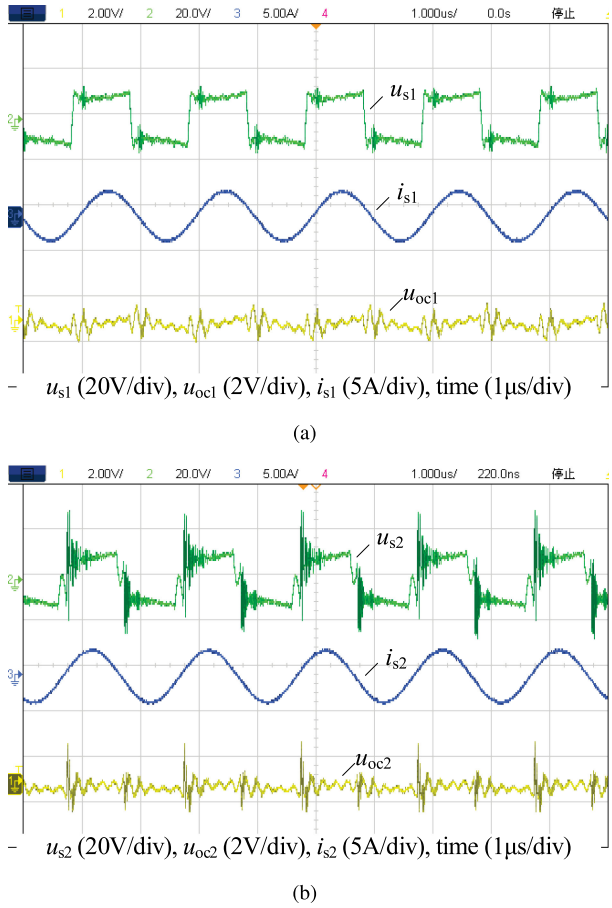

Fig. 22. Waveforms of measuring circuit for the same-side decoupling effect. (a) Primary side. (b) Secondary side.

P_1 denote the input voltage, current, and power, respectively. $U_{\rm dc2}$, $I_{\rm dc2}$, and P_2 indicate the output voltage, current, and power, respectively. The experimental result shows that the output power of the system is 1.51 kW, and the efficiency is 81.34%. Each inverter and rectifier carries about half of the total power.

Fig. 25 shows the experimental waveforms of the CPT system with the SISO coupler compared with the CPT system with the DIDO coupler. The parameters of the experimental setup are consistent with the theoretical analysis, e.g., the input voltage is 260 V, the dc load resistance is twice that of the proposed system, and the SISO coupler is composed of P_1, P_2, P_5, and P_6 in Fig. 20. In Fig. 25, the inverter current slightly lags behind the voltage, and the RMS values of primary current is 4.29 A, which is slightly less than the primary currents of 4.45 and 4.79 A in Fig. 23(a) and is consistent with the theoretical current relationship between the two systems shown in Fig. 16. In addition, the output dc voltage of the system in Fig. 25 is 236.1 V, which is slightly lower than the load voltage of 246.8 V shown in Fig. 23(b) and basically consistent with the transfer admittance relationship of the two systems shown in Fig. 15. In summary, comparing Figs. 23 and 25, it can be seen that the power of the CPT system with the DIDO coupler of 1.5 kW gives twice the output power of the CPT system with the SISO coupler

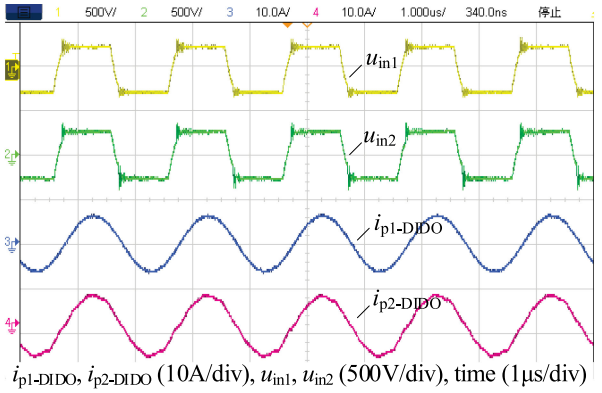

(a)

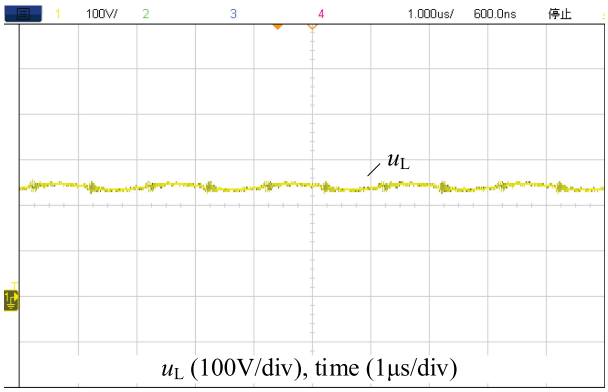

(b)

Fig. 23. Experimental waveforms of the CPT setup with the DIDO electric field coupler. (a) Output waveforms of two inverters. (b) Output voltage on the dc load.

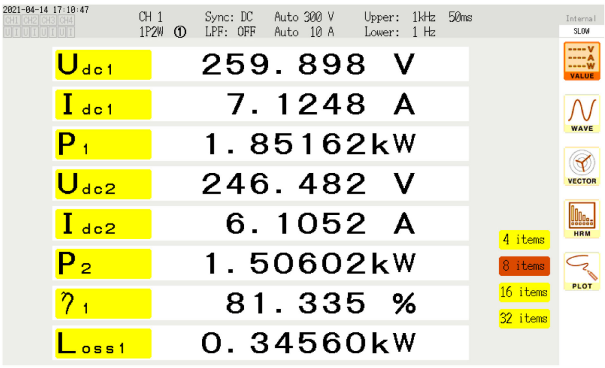

Fig. 24. Photograph of the power analyzer.

of 697 W, and the currents of the two systems are basically the same.

Fig. 26 shows the curves of the output current I_L and the efficiency η against the different load resistance R_L. According to (17), the output current of the system is independent of the load resistance R_L. In Fig. 26, as the load resistance increases from 15 to 60 Ω, the output current I_L remains approximately constant and slightly decreases from 3.72 to 3.36 A. The difference from the theoretical and experimental results is caused by the internal equivalent resistances of the components in the

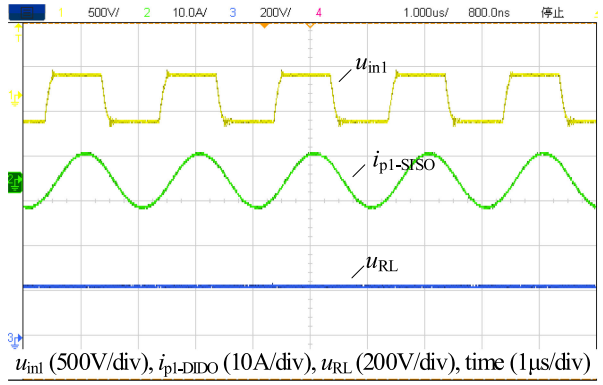

Fig. 25. Experimental waveforms of the CPT setup with the SISO electric field coupler.

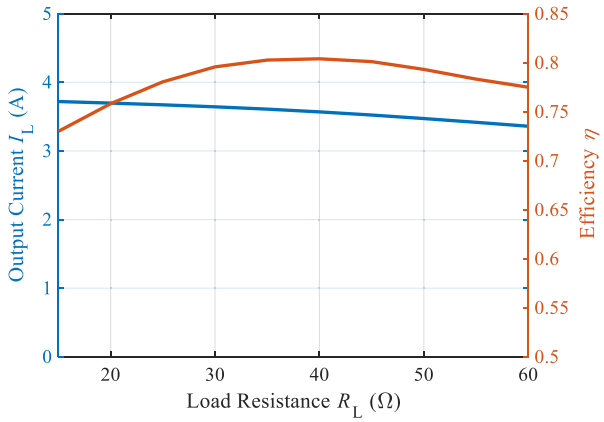

Fig. 26. Curves of system efficiency and output current against the load resistance.

experimental prototype. This phenomenon can be reproduced by adding internal resistance in the theoretical analysis. When the internal resistance of the circuit is not zero, the output current will decrease with the increase of load resistance, and it will become more serious when the internal resistances increase. The efficiency of the system is also a key factor. The efficiency curve in Fig. 26 first rises and then falls with the increase of the load resistance. The optimal efficiency point of 81.3% appears at the load resistance of 40 Ω.

Fig. 27 shows the power loss distribution of the proposed CPT system with a DIDO coupler. For all the compensation inductors, the loss includes core loss and winding loss. The core loss is calculated from datasheet of core and the current flowing through the core, and the winding loss is calculated according to the impedance of coils with the same length measured by the LCR meter and the current. For all the compensation capacitors, the power loss is calculated from the dissipation factor, the capacitance reactance, and the voltage of the capacitor. For the inverter and the rectifier, the loss is calculated from the relevant measured values from the experiment and the relevant parasitic parameters from the datasheet. Power losses other than the above parts are assumed to be the power losses on the coupler and other undefined items.

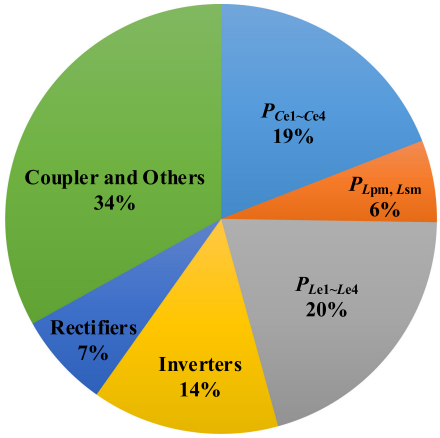

Fig. 27. Power loss distribution of the proposed CPT system.

VI. Conclusion

This article proposes a CPT system with extendable pairs of electric field couplers to enhance the power transfer capability by a modular approach. The complicated coupler is simplified as a circuit formed by CCVSs and self-capacitances in series by using a general model of an MIMO electric field coupler. Based on the simplified coupler circuit, the mutual capacitance on the same side of the coupler is found to be the cause of the detuning in the CPT system with an extendable coupler. A decoupling method based on shared inductances is proposed, and the analysis shows that when the shared inductance and the same-side mutual capacitance are fully tuned, the influence of the cross coupling on the system resonance will be eliminated. A 1.5-kW system with the DIDO coupler is built, and results show that the extended system with four pairs of coupling plates doubles the output power of the system with an SISO coupler by maintaining the same current ratings in the circuit. As a result, the effectiveness of the modular design approach is validated.

References

[1] J. Dai and D. C. Ludois, "A survey of wireless power transfer and a critical comparison of inductive and capacitive coupling for small gap applications," *IEEE Trans. Power Electron.*, vol. 30, no. 11, pp. 6017–6029, Nov. 2015.

[2] F. Lu, H. Zhang, and C. Mi, "A review on the recent development of capacitive wireless power transfer technology," *Energies*, vol. 10, no. 11, 2017, Art. no. 1752.

[3] X. Wu, Y. Su, A. P. Hu, X. Qing, and X. Hou, "Multiobjective parameter optimization of a four-plate capacitive power transfer system," *IEEE Trans. Emerg. Sel. Topics Power Electron.*, vol. 9, no. 2, pp. 2328–2342, Apr. 2021.

[4] Z. Liu, Y.-G. Su, Y.-M. Zhao, A. P. Hu, and X. Dai, "Capacitive power transfer system with double T-type resonant network for mobile devices charging/supply," *IEEE Trans. Power Electron.*, vol. 37, no. 2, pp. 2394–2403, Feb. 2022.

[5] R. Sedehi *et al.*, "A wireless power method for deeply implanted biomedical devices via capacitively coupled conductive power transfer," *IEEE Trans. Power Electron.*, vol. 36, no. 2, pp. 1870–1882, Feb. 2021.

[6] J.-Q. Zhu, Y.-L. Ban, R.-M. Xu, and C. C. Mi, "An NFC-connected coupler using IPT-CPT-combined wireless charging for metal-cover smartphone applications," *IEEE Trans. Power Electron.*, vol. 36, no. 6, pp. 6323–6338, Jun. 2021.

[7] C. Park *et al.*, "Separated circular capacitive coupler for reducing cross-coupling capacitance in drone wireless power transfer system," *IEEE Trans. Microw. Theory Techn.*, vol. 68, no. 9, pp. 3978–3985, Sep. 2020.

[8] S. Hagen, M. Tisler, J. Dai, I. P. Brown, and D. C. Ludois, "Use of the rotating rectifier board as a capacitive power coupler for brushless wound field synchronous machines," *IEEE Trans. Emerg. Sel. Topics Power Electron.*, to be published, doi: 10.1109/JESTPE.2020.3039497.

[9] *Wireless Power Transfer for Light-Duty Plug-in/Electric Vehicles and Alignment Methodology*, SAE Standard J2954, 2020.

[10] *Electric Vehicle Wireless Power Transfer—Part 1: General Requirements*, Standard GB/T-38775, 2020.

[11] Y. Li, R. Mai, L. Lu, and Z. He, "A harmonic elimination and power regulation approach of a cascaded multilevel technology in IPT systems," *Proc. Chin. Soc. Elect. Eng.*, vol. 20, no. 35, pp. 5278–5285, 2015.

[12] Y. Li, R. Mai, M. Yang, and Z. He, "Cascaded multi-level inverter based IPT systems for high power applications," *J. Power Electron.*, vol. 6, no. 15, pp. 1508–1516, 2015.

[13] Q. Deng, J. Liu, D. Czarkowski, W. Hu, and H. Zhou, "An inductive power transfer system supplied by a multiphase parallel inverter," *IEEE Trans. Ind. Electron.*, vol. 64, no. 9, pp. 7039–7048, Sep. 2017.

[14] Q. Deng, P. Sun, W. Hu, D. Czarkowski, M. K. Kazimierczuk, and H. Zhou, "Modular parallel multi-inverter system for high-power inductive power transfer," *IEEE Trans. Power Electron.*, vol. 34, no. 10, pp. 9422–9434, Oct. 2019.

[15] Y. Li, T. Lin, R. Mai, L. Huang, and Z. He, "Compact double-sided decoupled coils-based WPT systems for high-power applications: Analysis, design, and experimental verification," *IEEE Trans. Transp. Electrific.*, vol. 4, no. 1, pp. 64–75, Mar. 2018.

[16] Y. Li *et al.*, "Efficiency analysis and optimization control for input-parallel output-series wireless power transfer systems," *IEEE Trans. Power Electron.*, vol. 35, no. 1, pp. 1074–1085, Jan. 2020.

[17] U. K. Madawala and D. J. Thrimawithana, "Modular-based inductive power transfer system for high-power applications," *IET Power Electron.*, vol. 7, no. 5, pp. 1119–1126, 2012.

[18] W. Zhou, Z. Zhu, R. Mai, and Z. He, "Design and analysis of decoupled tetra-polar ring-coils for wireless power transfer in rotary mechanism applications," *IET Electr. Power Appl.*, vol. 14, no. 10, pp. 1766–1773, 2020.

[19] Y. Li, R. Mai, L. Ma, and Z. He, "Dual parallel wound primary coils based IPT systems and its power allocation technique," *Proc. Chin. Soc. Elect. Eng.*, vol. 17, no. 35, pp. 4454–4460, 2015.

[20] R. Mai, Y. Luo, B. Yang, Y. Song, S. Liu, and Z. He, "Decoupling circuit for automated guided vehicles IPT charging systems with dual receivers," *IEEE Trans. Power Electron.*, vol. 35, no. 7, pp. 6652–6657, Jul. 2020.

[21] Y. Liu, R. Mai, D. Liu, Y. Li, and Z. He, "Efficiency optimization for wireless dynamic charging system with overlapped DD coil arrays," *IEEE Trans. Power Electron.*, vol. 4, no. 33, pp. 2832–2846, Apr. 2018.

[22] Q. Zhu, M. Su, Y. Sun, W. Tang, and A. P. Hu, "Field orientation based on current amplitude and phase angle control for wireless power transfer," *IEEE Trans. Ind. Electron.*, vol. 65, no. 6, pp. 4758–4770, Jun. 2018.

[23] W. Zhou, L. Huang, B. Luo, R. Mai, Z. He, and A. P. Hu, "A general mutual coupling model of MIMO capacitive coupling interface with arbitrary number of ports," *IEEE Trans. Power Electron.*, vol. 36, no. 6, pp. 6163–6167, Jun. 2021.

[24] B. Regensburger, S. Sinha, A. Kumar, J. Vance, Z. Popovic, and K. K. Afridi, "Kilowatt-scale large air-gap multi-modular capacitive wireless power transfer system for electric vehicle charging," in *Proc. IEEE Appl. Power Electron. Conf. Expo.*, 2018, pp. 666–671.

Wei Zhou (Member, IEEE) received the B.E. and Ph.D. degrees from the School of Automation, Chongqing University, Chongqing, China, in 2013 and 2018, respectively.

He was a Visiting Scholar with the Department of Electrical, Computer and Software Engineering, The University of Auckland, Auckland, New Zealand from 2016 to 2017. He is currently a Lecturer with the School of Electrical Engineering, Southwest Jiaotong University, Chengdu, China. His current research interests include wireless power transfer technologies.

Qiao Gao received the B.E. degree from the College of Nuclear Technology and Automation Engineering, Chengdu University of Technology, Chengdu, China, in 2020. He is currently working toward the master's degree with the School of Electrical Engineering, Southwest Jiaotong University, Chengdu.

His main research interests include capacitive power transfer.

Ruikun Mai (Senior Member, IEEE) received the B.Sc. and Ph.D. degrees in electrical engineering from the School of Electrical Engineering, Southwest Jiaotong University, Chengdu, China, in 2004 and 2010, respectively.

He is currently a Professor with the School of Electrical Engineering, Southwest Jiaotong University. His research interests include wireless power transfer and its application in railway systems, power system stability, and control.

Zhengyou He (Senior Member, IEEE) received the B.S. and M.S. degrees from Chongqing University, Chongqing, China, in 1992 and 1995, respectively, and the Ph.D. degree from Southwest Jiaotong University, Chengdu, China, in 2001.

Since 2002, he has been a Professor with the School of Electrical Engineering, Southwest Jiaotong University. He was a Visiting Scholar with Cornell University, NY, USA, from 2008 to 2009. His research interests include signal processing and information theory and its application in electrical power systems, and the application of wavelet transforms in power systems.

Aiguo Patrick Hu (Senior Member, IEEE) received the B.E. and M.E. degrees from Xi'an Jiaotong University, Xi'an, China, in 1985 and 1988, respectively, and the Ph.D. degree from the University of Auckland, Auckland, New Zealand, in 2001.

He was with the National University of Singapore, Singapore, for a semester as an Exchange Postdoctoral Research Fellow. He is currently a Full Professor with the Department of Electrical, Computer and Software Engineering, The University of Auckland. He has authored or coauthored more than 200 peer-reviewed journal and conference papers, with about 4500 citations, authored the first monograph on inductive power transfer technology, and contributed to four book chapters on wireless power transfer modeling and control, and electrical machines. His research interests include wireless or contactless power transfer systems and application of power electronics in renewable energy systems.

Dr. Hu was the recipient of the University of Auckland Vice-Chancellor's Funded Research and Commercialization Medal in April 2017.